Published as: *Cell Rep*. 2020 June 16; 31(11): 107779–107779.

Brain circuit of claustrophobia-like behavior in mice identified by upstream tracing of sighing

Peng Li[1,2,*], **Shi-Bin Li**[3], **Xuenan Wang**[2], **Chrystian D. Phillips**[2], **Lindsay A. Schwarz**[4,5], **Liqun Luo**[4], **Luis de Lecea**[3], **Mark A. Krasnow**[1,6,*]

[1]Department of Biochemistry and Howard Hughes Medical Institute, Stanford University, Stanford, CA, 94305

[2]Life Sciences Institute, Department of Biologic and Materials Sciences, and Department of Molecular and Integrative Physiology, University of Michigan, Ann Arbor, MI, 48109

[3]Department of Psychiatry and Behavioral Sciences, Stanford University, Stanford, CA, 94305

[4]Department of Biology and Howard Hughes Medical Institute, Stanford University, Stanford, CA, 94305

[5]Current address: Department of Developmental Neurobiology, St. Jude Children's Research Hospital, Memphis, TN, 38105

[6]Lead contact

SUMMARY

Emotions are distinct patterns of behavioral and physiological responses triggered by stimuli that induce different brain states. Elucidating the circuits is difficult because of challenges in interrogating emotional brain states and their complex outputs. Here we leverage the recent discovery in mice of a neural circuit for sighing, a simple, quantifiable output of various emotions. We show that mouse confinement triggers sighing, and this "claustrophobic" sighing, but not accompanying tachypnea, requires the same medullary NeuromedinB (NMB)-expressing neurons as physiological sighing. Retrograde tracing from the NMB-neurons identified 12 forebrain centers providing presynaptic input, including hypocretin (HCRT)-expressing lateral hypothalamic neurons. Confinement activates HCRT-neurons, and optogenetic activation induces sighing and tachypnea whereas pharmacologic inhibition suppresses both responses. The effect on sighing is mediated by HCRT directly on NMB-neurons. We propose this HCRT-NMB neuropeptide relay circuit mediates claustrophobic sighing, and activated HCRT neurons are a claustrophobia brain state that directly controls claustrophobic outputs.

[*]Corresponding authors: penglium@umich.edu, 734-647-0232;, krasnow@stanford.edu, 650-723-7191.

AUTHOR CONTRIBUTIONS

P.L. performed the immunostaining, rabies virus synaptic tracing, breathing monitor, optogenetic, chemogenetic, and pharmacologic experiments, and analyzed the data. L.d.L. provided the Hcrt-IRES-Cre mice and guidance on optogenetic experiments, and S.-B.L. performed and analyzed the fiber photometry experiment. P.L. and C.D.P. performed and analyzed the confinement experiments. X.W. and P.L. performed and analyzed the RNAscope experiments. L.A.S. and L.L. provided the guidance, equipment, and reagents for rabies virus synaptic tracing. P.L. and M.A.K. conceived and designed experiments, interpreted data, and wrote the manuscript. All authors edited the manuscript.

DECLARATION OF INTERESTS

The authors declare no competing interests.

INTRODUCTION

Although emotions impact almost every aspect of our daily lives and have fascinated scientists for millennia (Darwin, 1874; Knuuttila, 2004), they have proven difficult to dissect and hard even to define. A prevailing view is that an emotion is the behavioral and internal manifestations of a central brain state that is subjectively experienced as a “feeling” (Anderson and Adolphs, 2014). Although the sensory triggers of an emotion, as well as its behavioral outputs -- such as laughing, crying, and sighing -- are often readily recognized, the central brain states and other internal manifestations of emotions have been more elusive. And, because the subjective experiences some consider essential for an emotion can only be interrogated in cognizant humans, research has historically focused on human subjects. Hence, there have been great experimental challenges in defining the underlying neuronal circuits, and even the general organization of the circuits is still debated, such as whether the subjective feeling underlying an emotion is a cause (upstream) or consequence (downstream) of the external manifestations (James, 1884; Lange, 1885; Cannon, 1927; Schachter and Singer, 1962; Pankesepp, 1998; LeDoux, 2012; Anderson and Adolphs, 2014).

Animals have long been thought to experience states that are similar to human emotional states, which Darwin proposed are homologous (Darwin, 1874). Although it has not been possible to interrogate feelings associated with animal states, genetically tractable model organisms are now being used to explore the neural circuits underlying certain emotion-like states (“emotion primitives”) (Anderson and Adolphs, 2014). In this paper we elucidate the brain organization and circuitry of a claustrophobic-like state in mice, by tracing upstream from brainstem neurons that control one of its specific behavioral outputs -- sighing.

Sighing is a stereotyped augmented breath pattern that is induced by dozens of human emotional states including stress, sadness, helplessness, relief, and pleasure (Ramirez, 2014; Li and Yackle, 2017). It also occurs spontaneously in all mammals, typically every few minutes, reinflating collapsed alveoli and restoring maximal gas-exchange efficiency of the lung (Knowlton and Larrabee, 1946; McCutcheon, 1953; Reynolds, 1962). Recently, we identified a peptidergic circuit in the mouse brainstem (medulla) that controls these spontaneous (“basal”) sighs as well as “physiological” sighs triggered by hypoxia (Li et al., 2016). This core circuit for sighing comprises ~200 neurons that express the bombesin-like neuropeptides neuromedin B (NMB) and gastrin releasing peptide (GRP) in the retrotrapezoid nucleus/parafacial respiratory group (RTN/pFRG), which project to and activate ~200 neurons expressing their cognate receptors Nmbr and Grpr in the respiratory rhythm generator, the preBötzinger Complex (the preBötC), transforming normal (“eupneic”) breaths into sighs (Li et al., 2016).

Here we report that sighing is induced when mice are briefly placed in tight quarters, a standard mouse paradigm for non-invasively inducing innate stress responses. We show that this “claustrophobic” sighing, but not the accompanying tachypnea (rapid breathing), requires the same brainstem neurons as basal and physiological sighing. We use monosynaptic retrograde tracing to map forebrain centers that provide direct input to the Nmb-expressing neurons, and molecularly identify neurons in one of the mapped centers

(the lateral hypothalamic area, LHA) that are activated by confinement and that project to and directly control the Nmb-expressing neurons through a second peptidergic pathway. We propose that these LHA neurons represent a key node in the central emotional state of mouse claustrophobia, and that they directly control sighing and separately control tachypnea, movement, and presumably other external and internal manifestations of the claustrophobic state. The results suggest a modular organization of neural circuits of emotion that allows facile evolutionary diversification of emotions.

RESULTS

Confinement triggers sighing and tachypnea in mice

To explore the possibility of using mice as a model for emotional sighing, we investigated breathing responses in a number of mouse behavioral paradigms. Confinement in tight quarters (or “acute restraint”) is a common paradigm for inducing innate stress responses in rodents (Zimprich et al., 2014). We found that when a mouse was placed in a tight-fitting 50 ml (27 mm diameter) conical tube, its sigh rate immediately increased 2.8 ± 0.3 fold (n=6, Figures 1A and 1B). The effect on sighing persisted throughout the confinement and then rapidly returned to base line following release from the tube (Figure 1A). Respiratory rate was also increased during confinement (Figure 1C), although the effect on sighing was greater (Figure 1D). Increased sighing and respiratory rate were also observed when mice were placed in a larger (33 mm diameter) metal mesh tube (Figures S1A to S1C). In addition, we found that anesthetizing mice eliminated the effect of tube confinement on sighing, although it left intact the effect of physiological challenge with hypoxia (Figure S1D).

Tube confinement also induced intermittent bouts of movement throughout the confinement period (Figure S1E). Interestingly, most (80 ± 14 %) sighs occurred in conjunction with these bouts of movement (Figures S1E). To determine if these movements induce sighing (e.g., through increased oxygen demand) or if the movements were another, independent manifestation of confinement stress (e.g. “struggling” to escape), we carried out a similar experiment in which mice were pre-treated with the nicotinic acetylcholine receptor antagonist tubocurarine (“curare”), to block transmission at the neuromuscular junction. This prevented almost all bouts of movement during confinement, but it did not alter the effect of confinement on sighing (Figures S1E and S1F).

These results suggest that the observed respiratory responses to tube confinement are not due simply to physical constriction of breathing, impaired ventilation, or induced movements, but rather to the stress associated with confinement (see also below). Thus, confinement stress induces sighing, at least one other respiratory response (tachypnea), and bouts of movement (“struggling”), and these appear to be part of an innate behavioral response because none of the responses required prior training.

The *Nmb*-expressing neurons in the RTN mediate confinement-induced sighing

Our previous work showed that basal and hypoxia-induced sighing are mediated by partially overlapping bombesin-like neuropeptide pathways in the medulla, in which the NMB-

expressing and GRP-expressing neurons in the RTN project to and control the receptor-expressing neurons in the pre-Bötzinger Complex breathing pacemaker (the preBötC) (Li et al., 2016). To determine if confinement-induced sighing is mediated by the same peptidergic circuit, we first generated a bacterial artificial chromosome (BAC) transgenic Nmb-CreERT2 mouse, with CreERT2 inserted at the start codon of the *Nmb* locus (Figure 1E), to allow genetic manipulation of the *Nmb*-expressing neurons (Figures 1F and 1G; see Methods).

We then used the Nmb-CreERT2 mice to specifically silence the Nmb-expressing neurons during the confinement paradigm, by stereotactically injecting into the RTN the adenoassociated viral (AAV) chemogenetic vector AAV-DIO-hM4Di (Krashes et al., 2017) (Figures 1F and 1G). Following Cre-mediated recombination hM4Di receptor is expressed in the Nmb-expressing neurons, which in the presence of clozapine-n-oxide (CNO) hyperpolarizes and silences the neurons. In transgenic mice under free range control conditions, silencing of the Nmb-expressing neurons by systemic administration of CNO (1 mg/kg body weight) diminished basal sighing (Figure S2A), confirming the role of these neurons in physiological sighing established previously by pharmacological manipulation of the NMB pathway (Li et al., 2016) (see also below). CNO administration also diminished the sighing induced when mice were placed in the conical tube (Figure 1H). Thus, the Nmb-expressing RTN neurons also play an important role in confinement-induced sighing. The effects on sighing were specific as there was no effect of CNO-induced Nmb neuron silencing on basal respiratory rate or the tachypnea induced by confinement (Figures S2B and S2E; see below).

Twelve forebrain regions provide direct input to the Nmb-expressing sigh control neurons

To identify neuronal inputs to the NMB-expressing neurons that could directly activate these neurons and the downstream sigh control circuit during stress, we used rabies virus retrograde monosynaptic circuit tracing (Wickersham et al., 2007; Schwarz et al., 2015). The helper genes TVA receptor and rabies virus envelope glycoprotein were first expressed in *Nmb*-expressing neurons in a Cre-dependent manner by stereotactic injection of AAV-FLEx^{loxP}-TVA-mCherry and AAV-FLEx^{loxP}-G into the RTN/pFRG of Nmb-CreERT2 mice (Figures 2A and 2B). This enables the specific infection and monosynaptic spread of an EnvA-pseudotyped, glycoprotein-deleted, and GFP-expressing rabies virus (RVdG) from *Nmb*-expressing neurons. By serial sectioning, we identified twelve forebrain regions with GFP-labeled cells indicating direct presynaptic input to the *Nmb*-expressing neurons (Figures 2B and 2C).

The LHA is activated by confinement and is sufficient to induce sighing

Among the brain regions identified as presynaptic to *Nmb*-expressing neurons, we focused on lateral hypothalamus area (LHA) (Figure 2D), a heterogeneous brain region that has been implicated in stress as well as arousal, feeding, and motivation (Bonnavion et al., 2016). The LHA is also known to modulate autonomic functions including breathing (Burdakov et al., 2013). We first examined whether LHA neurons are activated in the confinement paradigm that induces sighing, by immunostaining for the immediate early gene product c-Fos that is expressed in many neurons following activation. Under control conditions, only a few

LHA neurons expressed c-Fos. However, 90 minutes after mouse placement in a conical tube, there was a 4-fold increase in the number of c-Fos-positive neurons scattered across the LHA, implying that these neurons are activated by confinement stress (Figures S3A and S3B).

To test whether activation of LHA neurons is sufficient to induce sighing, we first injected the GABA receptor antagonist bicuculline into the LHA of anaesthetized wild-type mice to disinhibit LHA neurons. This increased sighing 4 to 6-fold in the first 10 minutes (Figures 3A and 3C), and the effect persisted for 20 – 30 minutes (Figure 3A). Induced sighs displayed the classical waveform of sighs (Bendixen et al., 1964; Li et al., 2016): an initial inspiratory peak indistinguishable from a eupneic breath immediately followed by a second inspiratory peak (Figure 3B).

We also tested the effect of optogenetic activation of LHA neurons on breathing. AAV-hSyn-ChR2 was injected into the LHA of a wild-type mouse, and after 3–4 weeks to allow viral infection and expression of channelrhodopsin ChR2, the LHA neurons were activated by a blue light laser. Upon 5Hz or 10Hz (but not 1Hz) laser activation, the sigh rate acutely increased 4–10 fold (Figures 3E, 3F, and S3D to S3F), similar to the effect of LHA disinhibition (Figure 3C). In both the LHA disinhibition and optogenetic activation experiments, respiratory rate also increased following LHA activation (Figures 3D, and S3G to S3I), just as in the behavioral paradigm (Figure 1C).

We conclude that LHA neurons are activated by confinement, and that activation of LHA neurons is sufficient to induce at least two external manifestations of confinement stress: increased sighing and tachypnea.

Hypocretin-expressing LHA neurons mediate the effects on sighing

Because the LHA is a heterogeneous neuronal population, we next investigated what neuronal type in the LHA mediates confinement-induced sighing. Retrograde AAV-hSyn-EGFP injected into the RTN labeled both glutamatergic excitatory neurons and GABAergic inhibitory neurons in the LHA (65% *Slc17a6* (Vglut2) positive, 29% *Slc32a1* (Vgat) positive, 1.4% double positive, and 4.3% double negative, n=138 scored neurons). Both populations are also activated by tube confinement paradigm as shown by neurons positive for *c-Fos+* (61% *Slc17a6* (Vglut2) positive, 29% *Slc32a1* (Vgat) positive, 0.5% double positive, and 11% double negative, n=1431 scored neurons). To activate different subsets of LHA neurons, optogenetic activation was performed on various transgenic Cre-expressing mice 2–3 weeks after a Cre-dependent channelrhodopsin AAV vector (AAV-DIO-ChR2) was stereotactically injected into the LHA. Laser activation of LHA glutamatergic excitatory neurons in Vglut2-IRES-Cre mice was sufficient to induce sighing, mimicking the effect of activation of all LHA neurons (Figure 4A, and S4A to S4I). Conversely, activation of LHA GABAergic inhibitory neurons in Vgat-IRES-Cre mice decreased sighing, but not respiratory rate (Figures 4B, and S4J to S4R). These results suggest that Vglut2+ excitatory neurons in the LHA mediate the induction of sighing.

Hypocretin (*hcrt*), also known as orexin, encodes a neuropeptide precursor expressed in only a small subset of neurons in the brain, all located in the LHA (de Lecea et al., 1998;

Sakurai et al., 1998). These Vglut2+ neurons play roles in arousal, appetite, sleep, and stress (Giardino and de Lecea, 2014; Sakurai, 2014). To determine if these neurons also mediate the induction of sighing by confinement, we first used c-Fos immunostaining to test whether they were activated by confinement stress. We found that under the tube confinement paradigm the fraction of c-Fos+ Hcrt neurons increased 5-fold to nearly 30% of all HCRT LHA neurons (Figures 4D and 4E), and the fraction of *c-Fos+ Hcrt* neurons is more than half (56%) of *c-Fos+* LHA excitatory neurons (n=1147 *c-Fos* and *Vglut2* double labeled neurons). Live activity recording of GCaMP6f-expressing Hcrt neurons by fiber photometry also demonstrated increased activity of these neurons during tube confinement (Figures 4F and 4G).

We then optogenetically activated the *Hcrt*-expressing neurons by injecting AAV-DIO-ChR2 into the LHA of a Hcrt-IRES-Cre knock-in mouse line. Photoactivation at 5 or 10Hz (but not 1 Hz) increased sighing 3–10 fold (Figures 4C, and S5B to S5D), similar to the response to confinement stress and to activation of all LHA neurons or just the excitatory neurons described above. Thus, *Hcrt*-expressing neurons in the LHA are activated by confinement, and their optogenetic activation is sufficient to induce sighing.

Hypocretin-expressing LHA neurons control sighing directly through *Nmb*-expressing RTN neurons

The monosynaptic retrograde tracing experiments described above provided evidence for neuronal projections from LHA directly to *Nmb*-expressing neurons in the RTN. To validate the connection from LHA to RTN, we injected fluorescent retrobeads into the RTN and 5 days later found evidence of bead uptake and retrograde transport into LHA neurons (Figure S6A), at least some of which express *Hcrt* as shown by HCRT immunostaining (Figure 5A). 29% of retrogradely labeled LHA excitatory neurons (n=80 *Vglut2* and *Egfp* double labeled neurons) by AAVretro-hSyn-EGFP injected in the RTN are *Hcrt* positive. Conversely, stereotactic injection of a YFP-expressing AAV vector (AAV-hSyn1-eYFP) into the LHA showed that YFP-labeled LHA neuronal processes project to the RTN (Figure S6B). Double staining for HCRT and NMB confirmed that HCRT-expressing neurons project to the RTN/pFRG and demonstrated that HCRT-positive termini directly abut cell bodies of *Nmb*-expressing neurons (Figure 5B). Multiplex single molecule fluorescent in situ hybridization showed that the two hypocretin receptor genes *Hcrtr1* and *Hcrtr2* are selectively expressed in the RTN in *Nmb*-expressing neurons, with nearly all *Nmb*-expressing neurons expressing one or both receptors (54% *Hcrtr1 Hcrtr2* double-positive, 15% *Hcrtr1 alone, 18% Hcrtr2 alone*; n= 39; vs. 1.1% double-positive, 0.2% *Hcrtr1* alone and 1.4% *Hcrtr2* alone in *Nmb*-negative RTN/pFRG neurons; n= 914) (Figure 5C). We conclude that *Hcrt*-expressing neurons in the LHA directly project to the RTN, that they closely approach and may contact *Nmb*-expressing neurons, and that there is direct peptidergic signaling possibility between these two sets of neurons mediated by HCRT through its receptors HCRTR1 and HCRTR2.

To explore the functional significance of the identified neurons and peptidergic circuit, we first tested the effect of the selective HCRT receptor antagonist almorexant (ALM) in the emotional sighing assay. Breathing was monitored in mice placed in the conical tube, following oral administration of either ALM (100 mg/kg) or vehicle control. ALM

substantially reduced confinement sighing (Figures 5E and 5F), and a similar effect of systemic ALM was observed on sighing induced by LHA disinhibition in anaesthetized mice (Figure 5H). To specifically interrogate the HCRT signal to *Nmb*-expressing neurons in the RTN, ALM was stereotactically injected into the RTN of anaesthetized Hcrt-IRES-Cre mice that had AAV-DIO-ChR2 injected into the LHA three weeks earlier to express channelrhodopsin ChR2. The local administration of ALM into the RTN diminished sighing induced by optogenetic activation of *Hcrt*-expressing neurons expressing ChR2 (Figure 5I), similar to the effect of systemic ALM following LHA disinhibition (Figure 5H). Thus, HCRT signaling mediates the sighing response induced by confinement, by disinhibition of the LHA, or by direct optogenetic activation of *Hcrt*-expressing neurons, and the effect is mediated by HCRT action in the RTN.

A similar diminution of confinement-induced (Figure 1E), LHA-disinhibition-induced (Figure 5J), and HCRT-neuron-induced (Figure 5K) sighing was obtained by blocking NMB signaling, either by chemogenetic silencing of Nmb neurons (Figure 1E) or by injection of NMBR antagonist BIM 23042 directly into the preBötC (Figures 5J and 5K). We conclude that *Nmb*-expressing neurons in the RTN that project to the preBötC mediate sighing induced by confinement as well as by disinhibition of the LHA or direct optogenetic activation of LHA *Hcrt*-expressing neurons.

The Hypocretin-Nmb circuit functions specifically in confinement sighing

Although HCRT and NMB pathway inhibition had very similar effects on confinement-induced (“emotional”) sighing, as well as sighing induced by LHA HCRT neuron activation, inhibition of the pathways had different effects on physiological sighing. NMB neuron silencing inhibited both basal (Figure S2A) (Li et al., 2016) and confinement-induced sighing (Figure 1G), whereas HCRT antagonism inhibited confinement-induced sighing but had no effect on basal sighing (Figures 5E and 5F). Similarly, the NMB antagonist diminished hypoxia-induced sighing (10% O_2 balanced by N_2) as we previously showed (Li et al., 2016), whereas the HCRT antagonist had no effect on hypoxia-induced sighing (Figure 6A). Thus, the upstream HCRT pathway specifically mediates confinement sighing, whereas the downstream NMB pathway mediates all known forms of sighing, including basal and hypoxia-induced sighing as well as confinement sighing.

There was one other subtle but important way in which the results with HCRT and NMB inhibition differed: on the effect of confinement and LHA activation on respiratory rate. Whereas systemic antagonism of HCRT signaling blocked the tachypnea induced by confinement (Figure 6B) or by LHA disinhibition (Figure 6C), silencing of *Nmb*-expressing neurons or antagonism of NMBR signaling did not diminish these effects (Figures S2E and S7A). This implies that the tachypnea induced by confinement and by LHA and Hcrt neuron activation is mediated by some other set of downstream neurons besides the *Nmb*-expressing neurons. These other downstream targets reside outside the RTN because, although systemic antagonism of HCRT signaling inhibited induction of both sighing and tachypnea (Figures 5E to 5H, 6B, and 6C), local antagonism of HCRT signaling in the RTN affected only sighing (Figures 5I and 6D).

DISCUSSION

The results identify a neuropeptide brain circuit that controls a specific behavioral output of an animal “emotion” -- the claustrophobic stress induced by confinement in cramped quarters. Placement of mice in a tight-fitting tube activates hypocretin-expressing neurons in the LHA, and their optogenetic activation is sufficient to induce sighing and tachypnea, mimicking the natural claustrophobic response. These HCRT neurons project to and directly control the *Nmb*-expressing neurons in the RTN, which express hypocretin receptors *Hcrtr1* and *Hcrtr2*. Furthermore, the NMB pathway connecting RTN to preBötC, the output circuit that mediates basal and physiological (hypoxia-induced) sighing (Li et al., 2016), also mediates claustrophobic sighing, as antagonizing either hypocretin signaling in the RTN or Nmb signaling in the preBötC was sufficient to block the induced sighing. We propose that this Hcrt-Nmb neuropeptide relay circuit from LHA to preBötC, and on to respiratory pre-motor and motor neurons, is the central brain circuit controlling emotional sighing triggered by claustrophobic stress (Figure 7).

Our discovery of the central control circuit for a specific behavioral output of an emotional state has important implications for the organization and logic of emotional circuits. Each emotion is thought to be associated with a specific brain state, triggered by certain external and/or internal stimuli and manifest by specific patterns of behavioral and physiological responses (Anderson and Adolphs, 2014). How each emotional state is represented in the brain is not known, nor is how each state is triggered by specific external and internal stimuli or its role in the behavioral and physiological manifestations of the state and the associated subjective feelings (Kragel and LaBar, 2016). By tracing upstream from a small set of neurons that controls sighing, we identified Hcrt-neurons in the LHA among the direct presynaptic inputs. The Hcrt-neurons comprise a key node in the confinement stress circuit because they are activated by confinement (Winsky-Sommerer et al., 2014; Figure 4D and 4E), and their activation is sufficient to induce the characteristic suite of responses including sighing, other behavioral responses (e.g., movement (Adamantidis et al., 2007)) and physiological (tachypnea) and endocrine (Bonnavion et al., 2015) changes (Figure 7), whereas their inhibition diminishes such responses.

Activated LHA Hcrt neurons thus appear to represent a, or the, critical node in the brain state of claustrophobic stress, functioning as master regulators of this state by impinging on different sets of downstream neurons, each controlling a discrete manifestation of the state. One set of neurons directly downstream is the *Nmb*-expressing neurons in the RTN that mediate sighing. Another must be breathing center neurons outside the RTN that control respiratory rate, because the tachypnea induced by claustrophobic stress and activation of LHA *Hcrt*-expressing neurons was blocked by systemic injection of a HCRT antagonist (Figure 6C) but not by local injection in the RTN (Figure 6D). The *Hcrt*-expressing neurons also target other parts of the brain that presumably control other manifestations of claustrophobic stress such as struggling movements (Figure S1E), the endocrine response (Bonnavion et al., 2015), and perhaps even higher brain regions that underlie subjective feelings associated with the state (Peyron et al., 1998). Hcrt neurons are involved in arousal, appetite, sleep, and stress (Giardino and de Lecea, 2014; Sakurai, 2014), so further

investigation of their molecular and functional heterogeneity will be necessary to fully elucidate this multi-functional population.

These divergent neural outputs from a central node in the circuit explain how an emotion encompasses a wide range of seemingly unrelated but coordinately-controlled behavioral, physiological, and endocrine outputs. These ideas can now be tested by systematic mapping of the claustrophobic circuit including all direct outputs of these key nodal neurons, as well as their direct inputs to explore how this emotional state is triggered by sensory stimuli of tube confinement.

Many physiological responses and behaviors are shared by different emotional states. For instance, sighing is associated with dozens of different human emotions and conditions including positive valence states such as pleasure and relief, but also negative valence states such as disgust, disappointment, and anxiety (Ramirez, 2014; Li and Yackle, 2017). Rodents, too, sigh under different emotional conditions: they express a “sigh of relief” (Soltysik and Jelen, 2005) as well as the stress-induced sighs described here. Our circuit tracing upstream from the *Nmb*-expressing neurons revealed 11 other forebrain regions with neurons that directly converge on the core sigh control neurons in the RTN. Although these regions are not likely sufficient to induce sighing during confinement because the induced sighing is eliminated when the HCRT input is blocked, each of these sets of upstream neurons (or their combinations) may function as a central node in a control circuit underlying another emotional state that has sighing among its outputs, such as the “relief” center that triggers the sigh of relief (Figure 7). Such convergent organization of emotional circuits would explain how disparate emotional states can share some of the same manifestations.

The nodal organization of the claustrophobia circuit, coupled with the convergence of 11 other higher brain circuits on the same sigh control neurons in the claustrophobia circuit, suggests an appealing model for the evolution and diversification of emotional circuits. We expect that key nodes and the overall organization of emotional sigh circuits are conserved (Li and Yackle, 2017), in line with Darwin’s early observations (Darwin, 1874). This would explain why rodents and humans show similar respiratory responses when experiencing anxiety (Blechert et al., 2007; Carnevali et al., 2013), or relief (Soltysik and Jelen, 2005; Vlemincx et al., 2010). But we also expect that inputs and outputs can evolve by rewiring of a circuit, for example by species-specific loss or gain of downstream connections from node to output centers (LeDoux, 2012). In this way we imagine that nodes in a dozen different emotion circuits converged during evolution on the same Nmb-expressing neurons in the RTN, perhaps after these neurons were established for control of basal and physiological sighing for peak respiratory performance. Interestingly, hyperactive HCRT signaling, tachypnea, and excessive sighing have been associated with stress, anxiety, and panic disorders in human patients and other animal models (Johnson et al., 2010; Tobin et al., 1983; Lum, 1975), suggesting that at least aspects of the neuropeptide relay circuit described here have been conserved and could underlie pathological conditions.

STAR METHODS

RESOURCE AVAILABILITY

LEAD CONTACT—Further information and requests for resources and reagents should be directed to and will be fulfilled by the Lead Contact, Mark A. Krasnow (krasnow@stanford.edu).

MATERIALS AVAILABILITY STATEMENT

All unique reagents generated for this study are available from the Lead Contact upon request.

DATA AND CODE AVAILABILITY STATEMENT

The study did not generate any unique datasets or code.

EXPERIMENTAL MODEL AND SUBJECT DETAILS

Animals—All procedures were carried out in accordance with animal care standards in National Institutes of Health (NIH) guidelines, and approved by Stanford Institutional Animal Care and Use Committee or the University Committee on Use and Care of Animals at the University of Michigan. Mouse strains were maintained in the C57BL/6 genetic background. Adult mice (6–24 weeks old) of both sexes were used. To generate the bacterial artificial chromosome (BAC) transgene Nmb-CreERT2, a BAC recombineering protocol was used (http://ncifrederick.cancer.gov/research/brb/recombineeringInformation.aspx to insert a CreERT2 cassette into BAC RP23–82E1 at the ATG start codon of the *Nmb* gene (Fig. 1D), as we did previously to construct a Nmb-GFP BAC transgene (Li et al., 2016). In the Nmb-CreERT2 transgenic line, most Nmb-expressing neurons (82%) co-expressed Cre, as determined by RNAscope multiplex single molecule fluorescence in situ hybridization (n=83 scored *Nmb*-expressing neurons). Vglut2-IRES-Cre, Vgat-IRES-Cre (Vong et al., 2011), Hcrt-IRES-Cre (Giardino et al., 2018) and Nmb-GFP (Li et al., 2016) have been previously described.

METHOD DETAILS

Histology, immunostaining and *in situ* hybridization—For histology and immunostaining, mouse brains were harvested and fixed overnight in 4% paraformaldehyde then cryopreserved in 30% sucrose at 4°C overnight. The fixed tissue was embedded in optimum cutting temperature compound (OCT), then sectioned at 10 – 40 microns (Leica cryostat CM3050 S). For immunostaining, sections were rinsed with Phosphate-Buffered Saline (PBS) with Tween 20 (PBST, 0.1% Tween 20), blocked with 3% bovine serum (BSA) in PBST for 1 hr, then incubated with primary antibody overnight at 4°C. Sections were rinsed in PBST and incubated for 1 hour at room temperature with species-specific secondary antibodies. Primary antibodies were: chicken anti-GFP (Abcam 13970; 1:1000 dilution), rabbit anti-cFos (Abcam ab7963, 1:500 dilution), and goat anti-HCRT1 (Santa Cruz sc-8070; 1:200 dilution). Secondary antibodies were: Alexa Fluor 488-conjugated donkey anti-chicken (Jackson Immuno Research; 1:400 dilution), Cy3-conjugated donkey

anti-rabbit (Jackson Immuno Research; 1:400 dilution), and Alexa Fluor 488 or 647-conjugated donkey anti-goat (Thermo Fisher Scientific; 1:500 dilution).

For *in situ* mRNA hybridization, brains were harvested and embedded in OCT as above. Tissue blocks were sectioned (10 microns), fixed in 4% paraformaldehyde, dehydrated in an ethanol series, and treated with Pretreatment Reagent (Advanced Cell Diagnostics). Double fluorescent *in situ* assay was then performed using proprietary RNAscope technology with their *Hcrtr1, Hcrt2, Egfp, Hcrt, Slc17a6, Slc32a1, Cre and Nmb* probes (Advanced Cell Diagnostics).

Breathing monitoring and analysis—For awake animals, individual mice were placed in a 450 ml whole body plethysmography chamber (Buxco) at room temperature (22°C) in 21% O_2 (for normoxia) or 8% O_2 (for hypoxic challenge) balanced with N_2. Mice were allowed to acclimate for 15–20 minutes in the chamber before beginning plethymography data collection, with respiratory parameters determined using EMKA iOX2 software. Sighs were identified in plethysmography traces by their characteristic biphasic ramp, augmented flow in the second phase of the inspiratory effort and prolongation of expiratory time following the event, as previously described (Li et al., 2016). Sigh rate was binned across 4 minute windows with 1 minute steps.

For anesthetized mice, after full anesthetization was achieved ~30 minutes after intraperitoneal injection of 20% urethane in PBS at a dosage of 1.6 g/kg, the trachea was cannulated and connected to a respiratory flow head connected to a spirometer (AD Instruments) to monitor airflow during spontaneous breathing. Breathing data was acquired by PowerLab (AD Instruments) and analyzed by LabChart software (AD Instruments). After baseline breathing stabilized (10 – 20 minutes), the response to pharmacological challenges or photoactivation was tested. Anesthetized preparation is used because it eliminated variability in breathing from manipulation-induced struggle of the mouse.

Tube confinement assay—Baseline breathing behavior of each experimental mouse was monitored by plethysmography as described above for 15–20 minutes. Then, the mouse was transferred into a tube and immediately placed back in the plethysmography chamber for an additional 10–20 minutes to monitor breathing behavior. Confinement tubes were 50 ml clear conical tubes (Corning Life Science, 352098; 27 mm diameter) with 15 – 20 holes (5–8 mm diameter) drilled along the bottom and side of the tube for ventilation. For the larger, metal mesh tubes, a 23-gauge steel wire sheet (0.25 inch mesh) was shaped into a 33 mm diameter cylindrical tube. For anesthetized mice, 1.6 g/kg urethane was intraperitoneally injected into the animal ~30 minutes before tube confinement. Animal movement during the assay was recorded by a video camera and manually scored offline. To block muscle movement during the assay, mice were injected intraperitoneally with tubocurarine chloride (0.13mg/kg; Sigma, T2379) or vehicle (saline) 5 minutes before placement in the tube. For c-Fos experiments, mice were returned to their home cage for 15 and 90 minutes after removal from the tube to allow c-Fos to accumulate before the mouse was euthanized and analyzed by c-Fos *in situ* hybridization and immunostaining. Control mice were similarly handled but without tube confinement.

Stereotactic injection—Adult mice were anesthetized with isoflurane (3–4% for induction, 1.5% for maintenance) for retrobead and adeno-associated virus injections, or by intraperitoneal injection of ketamine (65 mg/kg) and xylazine (13 mg/kg) for rabies virus injections, or with urethane (1.6 g/kg) for pharmacological injections. Anesthetized mice were placed in a stereotactic instrument (David Kopf Instruments, Model 940), with body temperature maintained at 36°C using a feedback-controlled heating pad (Physitemp, TCAT-2LV). The following coordinates were used for injection: LHA, −1.40 mm posterior to bregma, −5.25 mm ventral from surface, ±0.95 mm from midline; RTN, −6.0 mm, −5.25 mm ventral from surface, ±1.3 mm from midline; preBötC, −6.85 mm, −4.65 mm ventral from surface, ±1.25 mm from midline. For retrobead and viral injections, animals were recovered from the stereotactic injection and subcutaneous injections of carprofen were administered (5 mg/kg) for pain alleviation.

Circuit tracing—For monosynaptic retrograde tracing using rabies-GFP (Schwarz et al., 2015), adult Nmb-CreER mice were anesthetized with isoflurane, then 500 nL of a 1:1 mixture of AAV8 CAG-FLEx^{loxP}-rabies glycoprotein and AAV5 CAG-FLEx^{loxP}-TVA:mCherry were stereotactically injected into the left RTN. Five days later, animals were injected intraperitoneally with tamoxifen (5mg/kg) three times over 5 days. Two weeks after the first tamoxifen injection, animals were anesthetized with ketamine (65 mg/kg) and xylazine (13 mg/kg). 300–500 nL of EnvA-pseudotyped rabies-GFP virus (RVdG) was injected into the same position using the procedure described above. After recovery, mice were housed in a Biosafety Level 2 facility for 4–5 days before harvesting and analysis as above. GFP positive cells were counted in every other section counterstained with DAPI.

For circuit tracing with AAVretro or retrobeads, adult mice were anesthetized with isoflurane and stereotactically injected with retrograde AAVrg-hSyn1-EGFP (Addgene) or retrobeads (Lumafluor) into the RTN. For AAVretro, mice were euthanized 3–4 weeks later and brain tissue was processed as described above. Serial sections were collected and processed for RNAscope for detecting *Egfp*, *Hcrt*, *Slc17a6,* and *Slc32a1*. For retrobeads, mice were euthanized five to seven days after injection and brain tissue was collected and processed for immunofluorescence. Retrobeads was detected by autofluorescence, and HCRT was detected by goat anti-HCRT1 antibody.

For tracing the processes of LHA neurons, 6–8 weeks old mice were anesthetized with isoflurane and stereotactically injected into LHA region with AAV-hSyn1-eYFP (Stanford Vector Core). Two weeks later, the animal was euthanized and brain tissue was collected and sectioned. Fluorescent signal was imaged on RTN sections.

Optogenetics—For optogenetic manipulation of neuronal activity, channelrhodopsin-2 (ChR2) expressing AAVs: AAV-hSyn1-ChR2 and AAV-DIO-ChR2 viruses (Boyden et al., 2005) (Stanford Vector Core) were bilaterally injected into the LHA. Custom-built fibre connectors (fibre: 0.48 numerical aperture, 200 μm diameter; Thorlabs) were implanted 0.5 mm above the viral injection site. After 3–4 weeks recovery, the cannula was connected to a 473 nm laser for 1, 5, 10 or 20 Hz activation (15ms interval) for 4 minutes, and breathing was monitored was monitored by a flow head connected to the spirometer in urethane-anesthetized mice.

Chemogenetics—For chemogenetic manipulation of neuronal activity, AAV-DIO-hM4Di (Krashes et al., 2011) (University of North Carolina Viral Core) was stereotactically injected into RTN region of a Nmb-Cre mouse. After about 1 week recovery, 3 doses of tamoxifen (5mg/kg) were injected intraperitoneally to induce recombination over a period of 1 week. Two weeks after the first tamoxifen injection, CNO (1mg/kg) was injected intraperitoneally to activate hM4Di and 15 minutes later breathing data was collected by whole body plethysmography.

Fiber photometry—Fiber photometry was performed as described[41]. Briefly, 0.3 μl AAV vectors carrying genes encoding GCaMP6f (AAV-DJ-EF1α-DIO-GCaMP6f, Stanford Virus Core; AAV-DJ-EF1α-DIO-GFP was used as control) were injected to the LHA (AP: −1.35 mm, ML: +/− 0.95 mm, DV: −5.15 mm) of Hcrt-IRES-Cre mouse with a 5 μl Hamilton micro-syringe on a stereotaxic frame (Kopf Instruments). A glass fiber (400 μm in diameter, Doric Lenses, Franquet, Québec, Canada) for optical signal acquisition was then implanted with the tip at the injection site, and the implant was secured with dental cement and the mouse allowed to recover for at least two weeks. On the recording day, mice were connected to a flexible patch cord and habituated for two hours prior to GCaMP6f signal acquisition. GCaMP6f signal recording was done during the dark phase. Signal was initially recorded for 10 minutes as baseline in the home cage. The mouse was then put in a well-ventilated 50 ml clear conical tube (confinement paradigm) and placed in the home cage, then recorded for an additional10 minutes, released from the tube, and recorded for 10 additional minutes in the home cage. GCaMP6f signals were analyzed offline in Matlab using custom scripts. Peak counts of the GCaMP6f signal were determined by Matlab Prominence built-in features (https://www.mathworks.com/help/signal/ug/prominence.html), with peaks > mean value + 2* SD (standard deviation) based on all the detected peaks of GCaMP6f signal trace during each paradigm scored and quantified (see Fig. 4F and 4G). Peak frequencies prior to, during and after tube confinement were compared (paired t-test). GCaMP6f signal during animal transfer (at the 10–12 min and 20–22 min time windows) were excluded from analysis. In control mice expressing GFP instead of GCaMP6f, there was no activity-dependent fluorescent signal.

Pharmacology—For systemic antagonism of hypocretin signaling in awake animals, mice were gavage fed 100 mg/kg hypocretin receptor antagonist almorexant (ALM, Selleckchem) dissolved in 0.25% methylcellulose in PBS. After 2 hours, breathing behavior and response to tube confinement were monitored and recorded by plethysmography.

For anesthetized conditions, urethane was administered by intraperitoneal injection and breathing monitored through the tracheostomy tube as described above. For LHA disinhibition, 200 nl of GABA receptor antagonist bicuculline (Tocris, 1mM) was unilaterally injected into LHA of wild-type adult mice. To antagonize hypocretin signaling, animals were gavage fed ALM 2 hours before the bicuculline injection as described above.

For local pharmacological experiments combined with optogenetics, 2–4 weeks before the pharmacological injection AAV-DIO-ChR2 virus was injected into the LHA of Hcrt-IRES-Cre mice and a cannula implanted. To locally antagonize hypocretin signaling, 200 nl of ALM (20mM) was stereotactically injected into the RTN. Baseline breathing behavior

was recorded for 10 minutes before the response to photoactivation of hypocretin neurons was analyzed. To locally inhibit NMBR, 500 nl of NMBR antagonist BIM23042 (Tocris, 10uM) was stereotactically injected into the preBötC immediately before the response to photoactivation of hypocretin neurons was analyzed.

QUANTIFICATION AND STATISTICAL ANALYSIS

Data is presented as mean +/− standard error of the mean (SEM). Sample size (n) is specified in the figure legends. Student's t-test was used to analyze most of the results. For multiple comparisons, ANOVA was applied followed by post hoc t test. All the statistical details of experiments can be found in the result section. Differences in means were considered statistically significant at $p < 0.05$.

Supplementary Material

Refer to Web version on PubMed Central for supplementary material.

ACKNOWLEDGMENTS

We thank C. Guo (HHMI Janelia Farm) for assistance in generating the Nmb-CreER mouse, and M. He and B. Zhang (Advanced Cell Diagnostics) for assistance in RNAscope experiments. This work was supported by the Howard Hughes Medical Institute (M.A.K. and L.L.), and the University of Michigan startup funds, Walter V. and Idun Berry postdoctoral, and Parker B. Francis fellowships (P.L.). M.A.K. and L.L. are investigators of the Howard Hughes Medical Institute.

REFERENCES

Adamantidis AR, Zhang F, Aravanis AM, Deisseroth K, & Lecea LD (2007). Neural substrates of awakening probed with optogenetic control of hypocretin neurons. Nature, 450, 420–424. [PubMed: 17943086]

Anderson DJ, and Adolphs R (2014). A framework for studying emotions across species. Cell 157, 187–200. [PubMed: 24679535]

Bendixen HH, Smith GM, and Mead J (1964). Pattern of ventilation in young adults. J. Appl. Physiol. 1–4. [PubMed: 14104283]

Blechert J, Michael T, Grossman P, Lajtman M, and Wilhelm FH (2007). Autonomic and respiratory characteristics of posttraumatic stress disorder and panic disorder. Psychosom Med 69, 935–943. [PubMed: 17991823]

Bonnavion P, Jackson AC, Carter ME, and de Lecea L (2015). Antagonistic interplay between hypocretin and leptin in the lateral hypothalamus regulates stress responses. Nat Commun 6, 6266. [PubMed: 25695914]

Bonnavion P, Mickelsen LE, Fujita A, de Lecea L, and Jackson AC (2016). Hubs and spokes of the lateral hypothalamus: cell types, circuits and behaviour. The Journal of Physiology 594, 6443–6462. [PubMed: 27302606]

Boyden ES, Zhang F, Bamberg E, Nagel G, and Deisseroth K (2005). Millisecond-timescale, genetically targeted optical control of neural activity. Nat. Neurosci. 8, 1263–1268. [PubMed: 16116447]

Burdakov D, Karnani MM, and Gonzalez A (2013). Lateral hypothalamus as a sensor-regulator in respiratory and metabolic control. Physiology & Behavior 121, 117–124. [PubMed: 23562864]

Cannon WB (1927). The James-Lange theory of emotions: a critical examination and an alternative theory. The American Journal of Psychology 39, 106–124.

Carnevali L, Sgoifo A, Trombini M, Landgraf R, Neumann ID, and Nalivaiko E (2013). Different patterns of respiration in rat lines selectively bred for high or low anxiety. PLoS ONE 8, e64519. [PubMed: 23691240]

Darwin C (1874). The Expression of the Emotions in Man and Animals.

de Lecea L, Kilduff TS, Peyron C, Gao X, Foye PE, Danielson PE, Fukuhara C, Battenberg EL, Gautvik VT, Bartlett FS, et al. (1998). The hypocretins: hypothalamus-specific peptides with neuroexcitatory activity. Proc. Natl. Acad. Sci. U.S.a. 95, 322–327. [PubMed: 9419374]

Giardino WJ, and de Lecea L (2014). Hypocretin (orexin) neuromodulation of stress and reward pathways. Curr. Opin. Neurobiol. 29, 103–108. [PubMed: 25050887]

Giardino WJ, Eban-Rothschild A, Christoffel DJ, Li S-B, Malenka RC, de Lecea L, (2018). Parallel circuits from the bed nuclei of stria terminalis to the lateral hypothalamus drive opposing emotional states. Nat. Neurosci. 21, 1084–1095. [PubMed: 30038273]

James W (1884). What is an emotion? Mind 9, 188–205.

Johnson PL, Truitt W, Fitz SD, Minick PE, Dietrich A, Sanghani S, Träskman-Bendz L, Goddard AW, Brundin L, and Shekhar A (2010). A key role for orexin in panic anxiety. Nat. Med. 16, 111–115. [PubMed: 20037593]

Knowlton GC, and Larrabee MG (1946). A unitary analysis of pulmonary volume receptors. Am. J. Physiol. 1–15.

Knuuttila S (2004). Emotions in Ancient and Medieval Philosophy (Clarendon Press).

Kragel PA, and LaBar KS (2016). Decoding the Nature of Emotion in the Brain. Trends Cogn. Sci. (Regul. Ed.) 20, 444–455.

Krashes MJ, Koda S, Ye C, Rogan SC, Adams AC, Cusher DS, Maratos-Flier E, Roth BL, and Lowell BB (2011). Rapid, reversible activation of AgRP neurons drives feeding behavior in mice. J. Clin. Invest. 121, 1424–1428. [PubMed: 21364278]

LeDoux J (2012). Rethinking the emotional brain. Neuron 73, 653–676. [PubMed: 22365542]

Li P, Janczewski WA, Yackle K, Kam K, Pagliardini S, Krasnow MA, and Feldman JL (2016). The peptidergic control circuit for sighing. Nature 530, 293–297. [PubMed: 26855425]

Li P, and Yackle K (2017). Sighing. Curr. Biol. 27, R88–R89. [PubMed: 28171761]

Lum LC (1975). Hyperventilation: The tip and the iceberg. Journal of Psychosomatic Research.

McCutcheon FH (1953). Atmospheric respiration and the complex cycles in mammalian breathing mechanisms. J. Cell. Physiol. 41, 291–303.

Panksepp J (1998). Affective Neuroscience (Oxford University Press).

Peyron C, Tighe DK, van den Pol AN, de Lecea L, Heller HC, Sutcliffe JG, and Kilduff TS (1998). Neurons containing hypocretin (orexin) project to multiple neuronal systems. J. Neurosci. 18, 9996–10015. [PubMed: 9822755]

Ramirez J-M (2014). The integrative role of the sigh in psychology, physiology, pathology, and neurobiology. Prog. Brain Res. 209, 91–129. [PubMed: 24746045]

Reynolds LB (1962). Characteristics of an inspiration-augmentingreflex in anesthetized cats. J. Appl. Physiol. 1–6. [PubMed: 13881529]

Rosin DL, Chang DA, and Guyenet PG (2006). Afferent and efferent connections of the rat retrotrapezoid nucleus. J. Comp. Neurol. 499, 64–89. [PubMed: 16958085]

Sakurai T, Amemiya A, Ishii M, Matsuzaki I, Chemelli RM, Tanaka H, Williams SC, Richardson JA, Kozlowski GP, Wilson S, et al. (1998). Orexins and orexin receptors: a family of hypothalamic neuropeptides and G protein-coupled receptors that regulate feeding behavior. Cell 92, 573–585. [PubMed: 9491897]

Sakurai T (2014). The role of orexin in motivated behaviours. Nat. Rev. Neurosci. 15, 719–731. [PubMed: 25301357]

Schachter S, and Singer JE (1962). Cognitive, social, and physiological determinants of emotional state. Psychol Rev 69, 379–399. [PubMed: 14497895]

Schwarz LA, Miyamichi K, Gao XJ, Beier KT, Weissbourd B, DeLoach KE, Ren J, Ibanes S, Malenka RC, Kremer EJ, et al. (2015). Viral-genetic tracing of the input-output organization of a central noradrenaline circuit. Nature 524, 88–92. [PubMed: 26131933]

Soltysik S, and Jelen P (2005). In rats, sighs correlate with relief. Physiology & Behavior 85, 598–602. [PubMed: 16038951]

Teigen KH (2008). Is a sigh “just a sigh?” Sighs as emotional signals and responses to a difficult task. Scandinavian Journal of Psychology.

Tobin MJ, Chadha TS, Jenouri G, Birch SJ, Gazeroglu HB, and Sackner MA (1983). Breathing patterns. 2. Diseased subjects. Chest 84, 286–294. [PubMed: 6884104]

Vlemincx E, Van Diest I, Lehrer PM, Aubert AE, and Van den Bergh O (2010). Respiratory variability preceding and following sighs: a resetter hypothesis. Biol Psychol 84, 82–87. [PubMed: 19744538]

Vong L, Ye C, Yang Z, Choi B, Chua S, and Lowell BB (2011). Leptin action on GABAergic neurons prevents obesity and reduces inhibitory tone to POMC neurons. Neuron 71, 142–154. [PubMed: 21745644]

Wickersham IR, Finke S, Conzelmann K-K, Callaway EM, 2007. Retrograde neuronal tracing with a deletion-mutant rabies virus. Nat. Methods 4, 47–49. [PubMed: 17179932]

Wilhelm FH, Trabert W, and Roth WT (2001). Characteristics of sighing in panic disorder. Biol. Psychiatry 49, 606–614. [PubMed: 11297718]

Winsky-Sommerer R, Yamanaka A, Diano S, Borok E, Roberts AJ, Sakurai T, Kilduff TS, Horvath TL, and de Lecea L (2004). Interaction between the corticotropin-releasing factor system and hypocretins (orexins): a novel circuit mediating stress response. J. Neurosci. 24, 11439–11448. [PubMed: 15601950]

Zimprich A, Garrett L, Deussing JM, Wotjak CT, Fuchs H, Gailus-Durner V, de Angelis MH, Wurst W, and Hölter SM (2014). A robust and reliable non-invasive test for stress responsivity in mice. Front. Behav. Neurosci. 8, 125. [PubMed: 24782732]

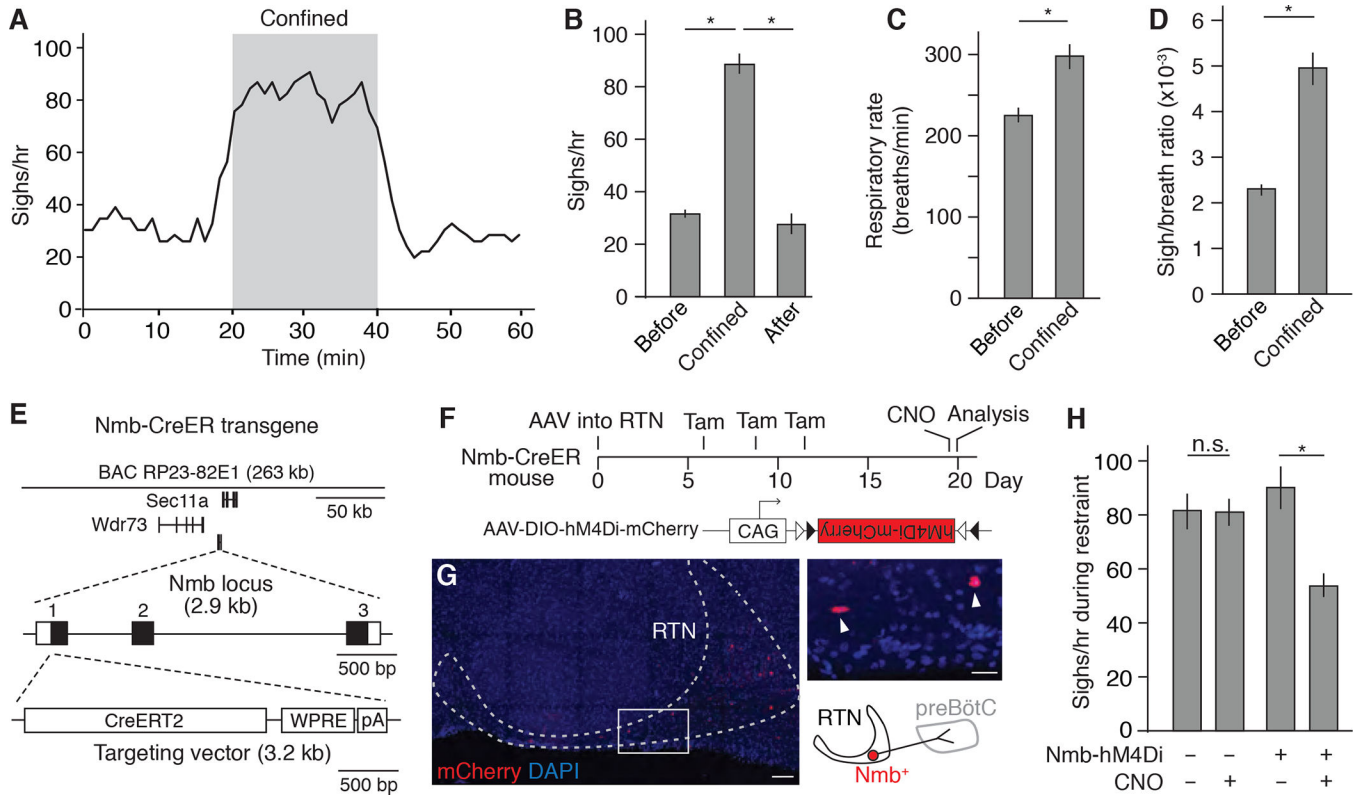

Figure 1. Tube confinement induces sighing through *Nmb* neurons in RTN.

(A) Sigh rate (bin 4 min, slide 1 min) determined by plethysmography of wild-type C57BL/6 mice (n=6) before, during, and after placement in a 50 ml conical tube. Grey, confinement period. (B) Quantification of sigh rate before, during, and after tube confinement (mean +/− SEM). *, p<0.05 (ANOVA followed by post hoc t-test). (C and D) Quantification of respiratory rate (C) and sigh-to-eupneic-breath ratio (D) before and during tube confinement (mean +/− SEM). *, p<0.05 (paired t-test). (E) Map of Nmb-CreERT2 mouse BAC transgene used for marking and manipulating Nmb-expressing sigh control neurons in medulla retrotrapezoid nucleus (RTN). The three exons of the Nmb locus are numbered (black fill, coding region). WPRE, Woodchuck Hepatitis Virus (WHP) Posttranscriptional Response Element; pA, polyadenylation signal. (F) Scheme for chemogenetic silencing of Nmb-positive RTN neurons. RTN of Nmb-CreERT2 adult mouse is infected with recombinant AAV-DIO-hM4Di-mCherry virus. Expression of CNO-dependent neuronal silencer hM4Di and mCherry is induced by tamoxifen (Tam), and then hM4Di is activated by CNO. CAG, cytomegalovirus early enhancer/chicken beta actin promoter; triangles, Cre recombination sites. (G) Expression of mCherry (red) in Nmb-CreERT2-expressing neurons in RTN (dashed outline) at day 20 of scheme in F. DAPI (nuclear marker), blue. Inset, close up of boxed region showing two labeled *Nmb*-expressing neurons (arrowheads) and schematic diagram of one of them. Scale bar, 100 um (50 um, inset). (H) Sigh rate during tube confinement in mice with (+, n=6) and without (−, n=5) hM4Di expression in *Nmb* neurons (Nmb-hM4Di) treated with (+) or without (−, vehicle only) CNO injection as shown in F. Note the residual sighing during confinement could

due to incomplete silencing of *Nmb* neurons or to *Grp* neurons in RTN, which have similar function. *, $p<0.05$; n.s., not significant.

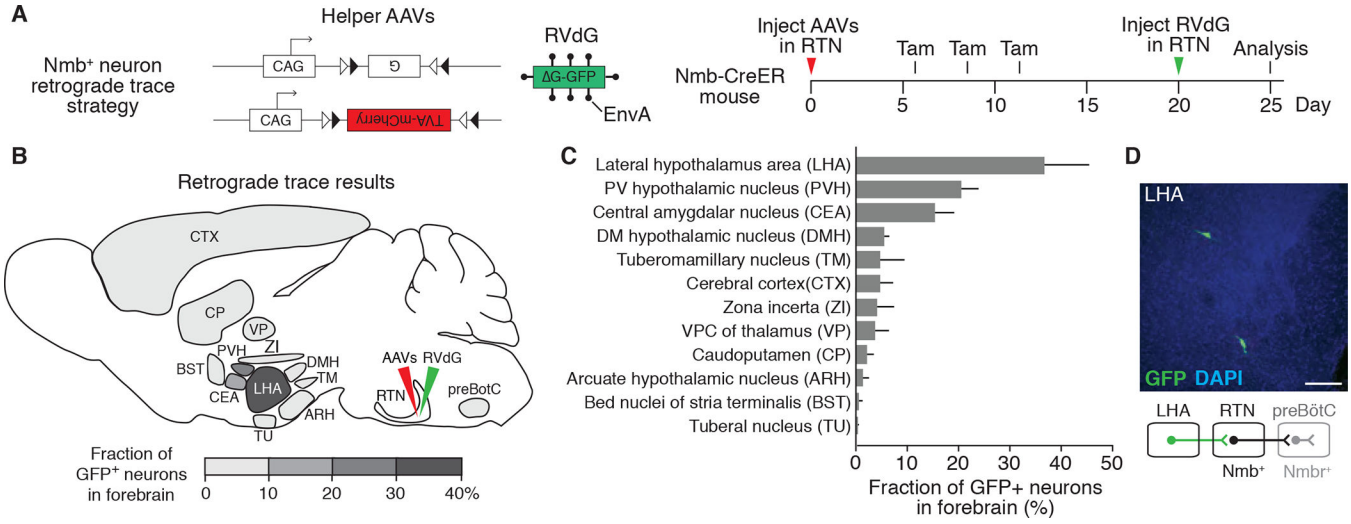

Figure 2. Mapping the direct forebrain inputs to RTN *Nmb* neurons by monosynaptic retrograde tracing.

(A) Scheme for rabies virus monosynaptic retrograde tracing of inputs to *Nmb* neurons. Two Cre-dependent helper AAVs (CAG-FLEx^{loxP}-rabies glycoprotein, top, and CAG-FLEx^{loxP}-TVA:mCherry, bottom) were injected into RTN (see B) of Nmb-CreER mouse, followed by intraperitoneal tamoxifen (Tam) injections to express in Nmb-CreERT2-expressing neurons the rabies glycoprotein (G) and the TVA receptor for EnvA fused to mCherry. After injection of EnvA-pseudotyped, glycoprotein deleted and GFP-expressing rabies virus (RV*d*G) to the same region (RTN), direct inputs to Nmb neurons are labeled. Open and closed triangles, Cre recombination sites. (B and C) Quantification of forebrain regions labeled by monosynaptic retrograde tracing in A that provide direct input to RTN *Nmb* neurons. Locations of labeled regions are density-coded in B to show relative abundance of labeling. DMH, dorsomedial hypothalamic nucleus; PVH, paraventricular hypothalamic nucleus; VPC, ventral posterior complex. Mean +/−SEM, n=3. (D) Coronal section (30 um) of mouse brain showing two rabies-labeled GFP-positive neurons in LHA region and a schematic below of their projection (green) from LHA to RTN. preBötC, preBötzinger Complex. Scale bar, 100 um.

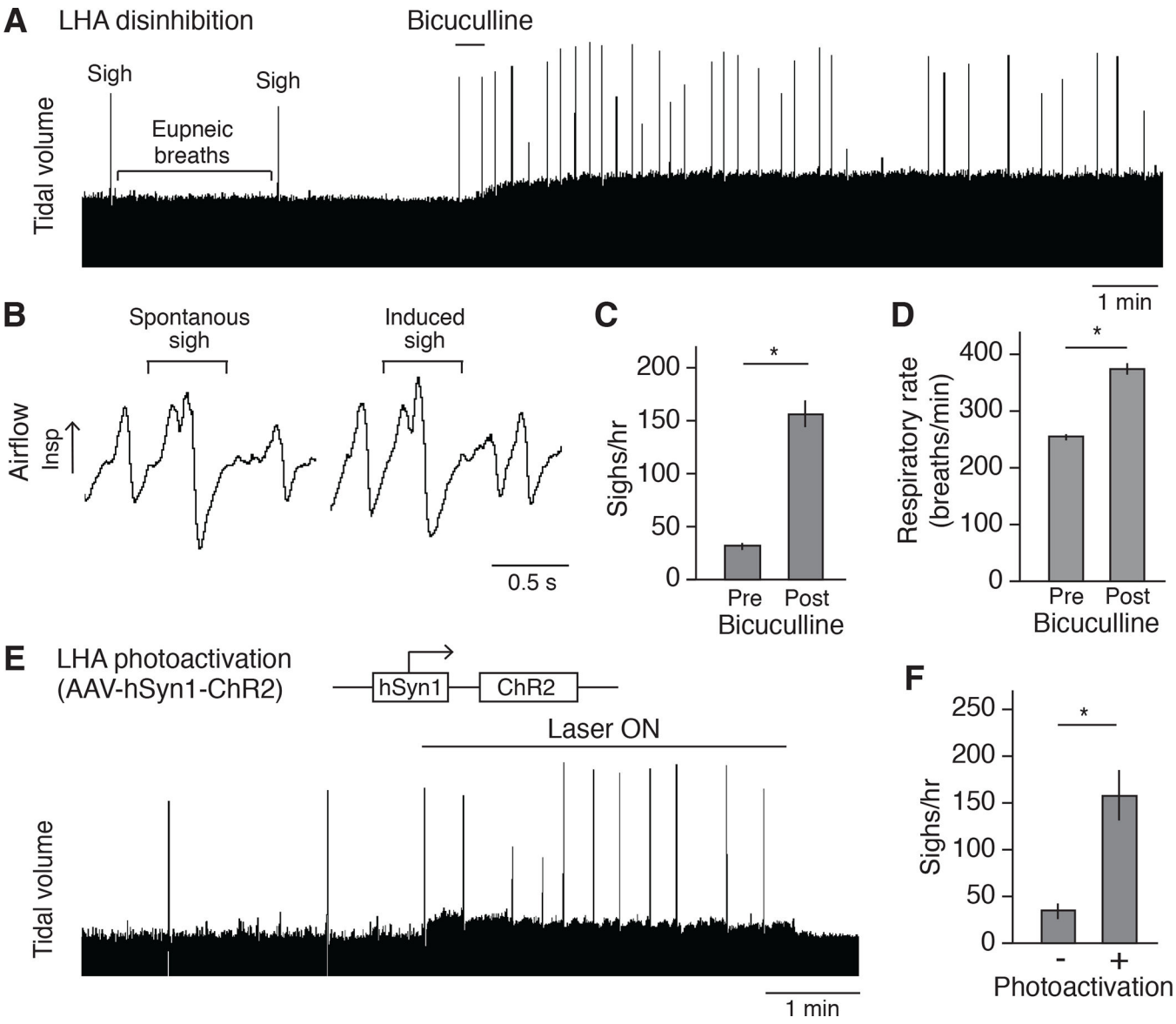

Figure 3. Activation of LHA neurons induces sighing.

(A) Respiratory trace (~15 minutes) showing respiratory activity of an anesthetized wild-type C57BL/6 mouse before and after stereotactic bicuculline injection to disinhibit LHA. Note standard (eupneic) breaths are normally punctuated every few minutes by a double-size sigh, which increase in frequency after bicuculline injection. Also note that the tidal volume is increased after disinhibition. Because the tidal volume is harder to quantify reliably for the confinement experiment in behaving animals by plethysmography, no further characterization was performed on tidal volume. Scale bar, 1 min. (B) Expanded trace segments showing similarity of sigh waveform before (spontaneous sigh) and after (induced sigh) bicuculline injection. Scale bar, 0.5 second. (C and D) Quantification showing sigh rate (C) and respiratory rate (D) of wild-type mice (n=6, mean +/−SEM) before (pre) and after (post) bicuculline injection. *, $p<0.05$ (paired t-test). (E) Plethysmography trace of anesthetized wild-type mouse stereotactically injected in LHA with the optogenetic

AAV diagrammed 2 weeks earlier to express chanelrhodopsin ChR2, then photoactivated with fiberoptic laser at 5 Hz. (F) Quantification of sigh rate of wild-type mice with photoactivation of LHA as in e (mean +/−SEM, n=6; *, $p<0.05$, paired t-test).

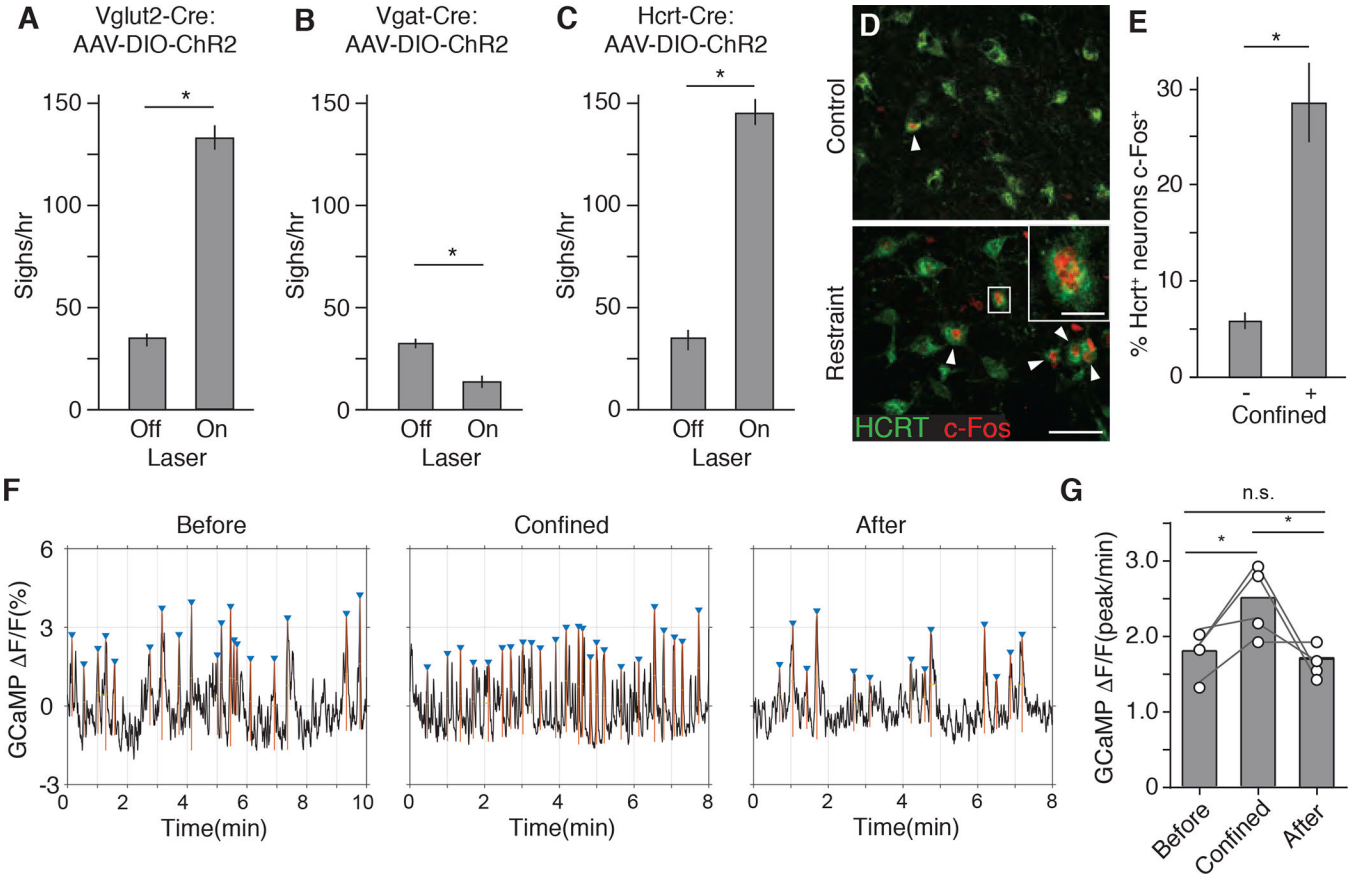

Figure 4. Hypocretin-expressing LHA neurons are activated by confinement and induce sighing.

(A to C), Sigh rate of anesthetized adult Vglut2-IRES-Cre (A), Vgat-IRES-Cre (B), and Hcrt-IRES-Cre (C) knock-in mice (mean +/−SEM, n=6 mice per condition) stereotactically injected with AAV-DIO-ChR2 into LHA, then photoactivated 2 weeks later with a blue laser for 4 min at 5 Hz (A and C) or 10 Hz (B) to optogenetically activate the indicated LHA neurons and analyzed by spirometer. (D) LHA brain sections of adult wild-type mice immunostained for HCRT1 (green) and neural activity marker c-Fos (red) 1.5 hours after mock handling (upper panel) or tube confinement (lower panel) for 15 min. Arrowheads, HCRT1/c-Fos double-positive neurons. Inset, close up of boxed region showing a double-positive neuron. Scale bar, 50 um (inset, 10 um). (E) Quantification of D showing percentage of HCRT1^{+} LHA neurons that co-stained for c-Fos (c-Fos^{+}) (mean +/−SEM, n=511 neurons scored in 4 animals *, $p<0.05$, unpaired t-test). (F) Hcrt neuron activity before, during, and after tube confinement measured by fiber photometry of GCaMP6f fluorescence (ΔF/F) in the LHA of AAV-DJ-EF1α-DIO-GCaMP6f-infected Hcrt-IRES-Cre mice. Triangles, GCaMP6f fluorescence peaks (calcium spikes) defined as >80% of difference between maximum and minimum values of GCaMP6f signal trace. (G) Quantification of GCaMP6f fluorescence peaks in **f** (n=4 mice; *, $p<0.05$, paired t-test).

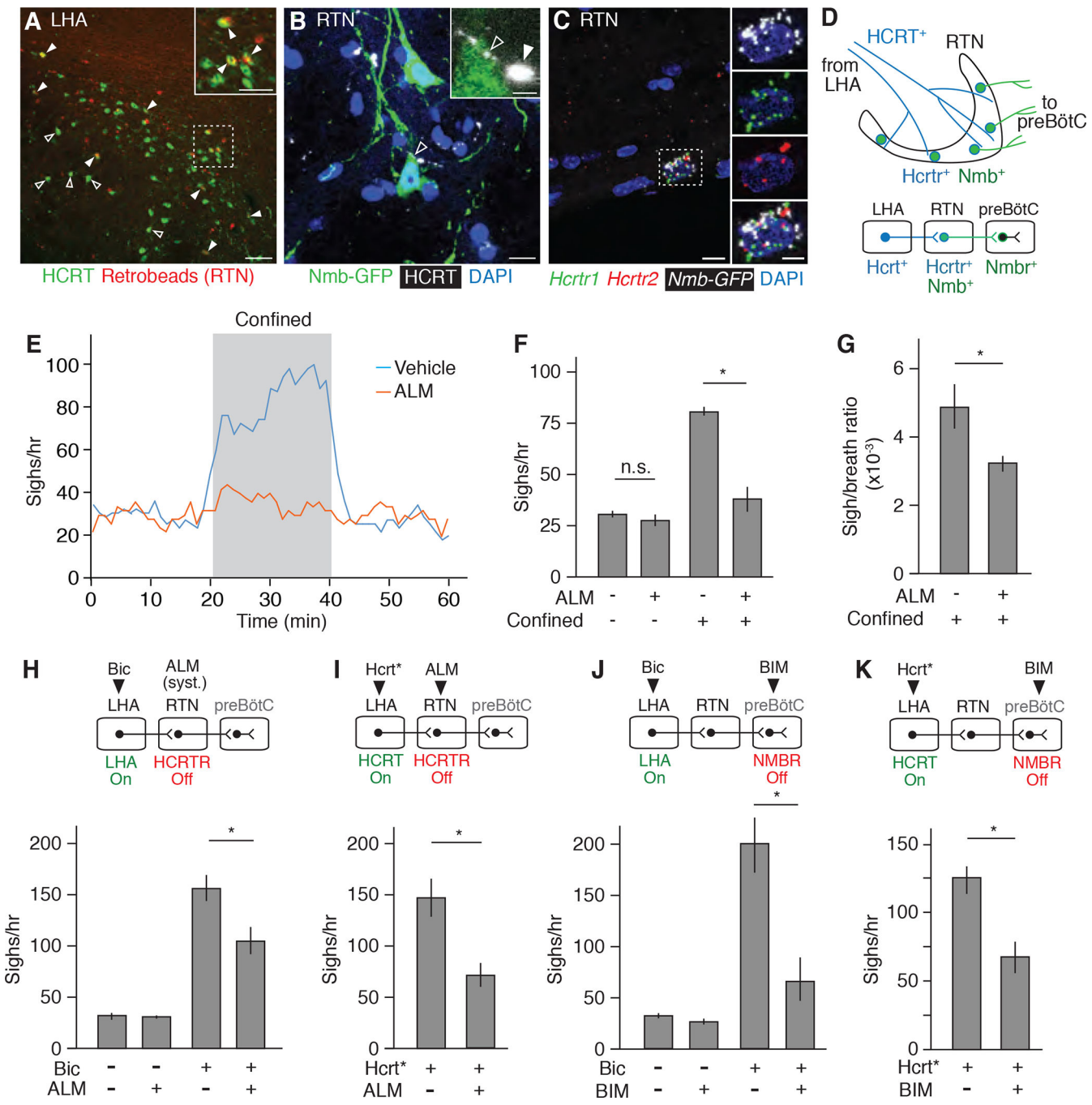

Figure 5. The HCRT neuropeptide pathway controls confinement-induce sighing through Nmb neurons.

(A) LHA brain slice of adult mouse injected in RTN with fluorescent retrograde tracer (retrobeads, red) then immunostained for HCRT1 (green) 5 days later. Arrowheads, HCRT1+ neurons co-stained with retrobeads, indicating projection to RTN; the retrobead (red) signal for some co-stained neurons (open arrowheads) is obscured by the strong HCRT signal (green) in image shown but readily detected when red and green channels are split (not shown). Inset, close-up of boxed region. Scale bars, 100 um (50 um, inset). (B) RTN region of adult Nmb-GFP BAC transgenic mouse immunostained for GFP (green) and

HCRT1 (white pseudocolor). Open arrowhead, HCRT1 puncta in axon directly abutting Nmb-GFP positive neuron (green); inset shows close-up. Filled arrowhead, HCRT1 puncta close though not abutting Nmb-GFP positive neuron (green). Scale bar, 10 um (2 um, inset). (C) Multiplex single molecule in situ hybridization (RNAscope) of RTN region probed for *Hcrtr1* (green), *Hcrtr2* (red) and *Egfp* (white pseudocolor) transcripts. Note isolated Nmb-GFP+ neuron co-expressing both receptors (boxed, enlarged in right panels that show split channels). Scale bar, 10 um (5 um, inset). (D) Diagram (upper) and schematic (lower) of A to C showing HCRT+ processes (blue) from LHA projecting to *Nmb*-expressing neurons in RTN (green) that co-express *Hcrt receptors Hcrtr1* and *Hcrtr2* and project to *Nmbr*-expressing neurons in preBötC. (E) Sigh rate before, during, and after tube confinment of awake, behaving wild-type mice (bin 4 min, slide 1 min) gavage fed with 100 mg/kg HCRTR antagonist almorexant (ALM, red; n=7) or vehicle (blue; n=8) 2 hours before plethysmography. Grey, confinement period. (F and G) Quantification of e showing sigh rate (F) and sigh-to-eupneic-breath ratio (G) of ALM-treated (+, n=7) and vehicle control (−, n=8) animals before (−) and during (+) confinement. Data as mean +/−SEM; *, $p<0.05$ (unpaired t-test). (H) Sigh rate before (−) and after (+) stereotactic bicuculline (Bic) injection to de-repress (activate) LHA of anesthetized mice treated systemically with ALM (+) or vehicle control (−) 2 hours before plethysmography. Experimental scheme is diagrammed above graph. Note reduction in LHA-induced sighing by systemic (syst.) HCRTR antagonism. n=6 per condition. (I) Sigh rate during optogenetic LHA Hcrt-IRES-Cre neuron activation (Hcrt*, Fig. 4C) of anesthetized mice injected in RTN with ALM (+, n=7) or vehicle control (−, n=5). Note reduction in Hcrt neuron-induced sighing by HCRTR antagonism in RTN. (J) Sigh rate before (−) and after (+) bicuculline injection to de-repress LHA of anesthetized mice with NMBR antagonist BIM23042 (+, n=7) or vehicle (−, n=6) injected in preBötC. Note reduction in LHA-induced sighing by NMBR antagonism in preBötC. (K) Sigh rate during optogenetic LHA *Hcrt-IRES-Cre* neuron activation of anesthetized mice with BIM23042 (+) or vehicle (−) injected into preBötC. Note reduction in HCRT neuron-induced sighing by NMBR antagonism in preBötC. n=6 per condition. For H to K, mean +/−SEM; *, $p<0.05$ (unpaired t-test).

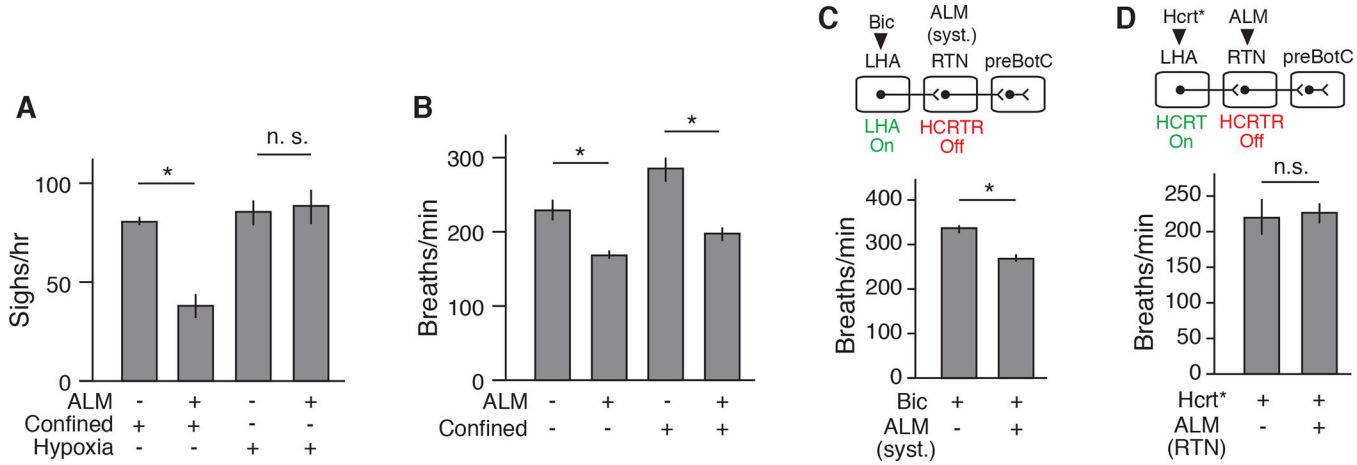

Figure 6. Specificity of HCRT-NMB circuit for confinement-induced sighing.

(A) Sigh rate of wild-type adult mice under tube confinement or hypoxia (10 % O_2) that were gavage fed with HCRTR antagonist ALM (+) or vehicle (−) for 2 hours before plethysmography. Note systemic HCRTR antagonism diminished confinement-induced but not hypoxia-induced sighing. Mean +/−SEM; sample size n=3; *, $p<0.05$ (unpaired t-test). (B) Respiratory rate before (−) and during (+) confinement of mice systemically treated with ALM (+, n=7) or vehicle (−, n=8) (Fig. 5 E to G). Note HCRTR antagonism reduced respiratory rate under basal and confinement conditions (mean +/−SEM; *, $p<0.05$, unpaired t-test). (C) Respiratory rate after bicuculline injection to activate LHA of anesthetized mice systemically treated 2 hours earlier with ALM (+, n=7) or vehicle (−, n=6) (Fig. 5H). Note HCRTR antagonism reduced tachypnea induced by pharmacologic LHA activation (mean +/−SEM; *, $p<0.05$, unpaired t-test). (D) Respiratory rate during optogenetic activation of *Hcrt-IRES-Cre* neurons (Hcrt*) of anesthetized mice injected with ALM (+, n=7) or vehicle (−, n=5) in RTN (Fig. 5I). Note local HCRTR antagonism in RTN did not affect tachypnea induced by Hctr neuron activation in LHA (mean +/−SEM; *, n.s., not significant, unpaired t-test).

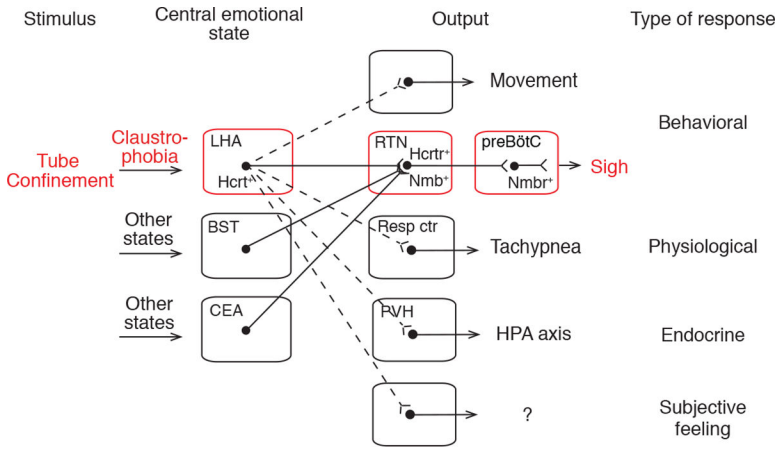

Figure 7. Model of the circuit organization of claustrophobia and its relation to other emotional circuits.

Tube confinement activates HCRT neurons in LHA, which directly activate Hcrtr+ Nmb+ double-positive neurons in RTN, which in turn project to and directly activate Nmbr+ neurons in the preBötC, comprising a neuropeptide “relay circuit” that triggers sighing. The LHA HCRT neurons represent a key node in the central emotional state of claustrophobic stress because they also activate other behavioral (struggling movements), physiological (tachypnea), and endocrine (hypothalamic-pituitary-adrenal axis, HPA axis) outputs, and perhaps subjective feelings through other targets (dashed lines). Other central emotional states (e.g., relief, sadness) are associated with activation of other brain regions, some of which (e.g., bed nuclei of stria terminalis, BST; central amygdalar nucleus, CEA) also project to the Nmb+ RTN neurons (solid lines) and induce sighing. Certain physiological states (e.g., hypoxia) also provide input to the Nmb+ RTN neurons (not shown). Resp ctr, respiratory center (not RTN); PVH, paraventricular hypothalamic nucleus.

KEY RESOURCES TABLE

REAGENT or RESOURCE	SOURCE	IDENTIFIER
Antibodies		
chicken anti-GFP	Abcam	Cat# ab13970, RRID:AB_300798
rabbit anti-cFos	Abcam	Cat# ab7963, RRID:AB_306177
goat anti-HCRTI	Santa Cruz	Cat# sc-8070, RRID:AB_653610
Donkey anti-chicken (Alexa Fluor 488)	Jackson ImmunoResearch Labs	Cat# 703–545-155, RRID:AB_2340375
Donkey anti-rabbit (Cy3)	Jackson ImmunoResearch Labs	Cat# 711–165-152, RRID:AB_2307443
Donkey anti-goat (Alexa Fluor 488)	Thermo Fisher Scientific	Cat# A-11055, RRID:AB_2534102
Donkey anti-goat (Alexa Fluor 647)	Thermo Fisher Scientific	Cat# A-21447, RRID:AB_2535864
Bacterial and Virus Strains		
AAV-CAG -FLEx^{loxP}-rabies glycoprotein	Schwartz et al., 2015	N/A
AAV-CAG-FLEx^{loxP}-TVA:mCherry	Schwartz et al., 2015	N/A
EnvA-pseudotyped rabies-GFP virus (RVdG)	Schwartz et al., 2015	N/A
AAV-hSyn1-ChR2	Stanford Vector Core	N/A
AAV-DIO-ChR2	Stanford Vector Core	N/A
AAV-DIO-hM4Di	University of North Carolina Viral Core	Cat#AV-5–52925
Chemicals, Peptides, and Recombinant Proteins		
Clozapine *N*-oxide (CNO)	Tocris Bioscience	Cat#4936; CAS: 34233–69-7
Tamoxifen	Sigma-Aldrich	Cat#T5648; CAS: 10540–29-1
Almorexant	Selleckchem	Cat#S2160; CAS: 913358–93-7
(-)-Bicuculline methiodide	Tocris Bioscience	Cat#2503; CAS: 40709–69-1
BIM 23042	Tocris Bioscience	Cat#3237; CAS:111857–96-6
Experimental Models: Organisms/Strains		
Mouse: C57BL/6	Jackson Laboratory	Stock #000664
Mouse: Vglut2-ires-Cre	Jackson Laboratory	Stock #016963
Mouse: Vgat-ires-Cre	Jackson Laboratory	Stock #016962
Mouse: Nmb-GFP	Li et al., 2016	N/A
Mouse: Nmb-CreERT2	This paper	N/A
Mouse: Hcrt-ires-Cre	de Lecea Laboratory	N/A
Software and Algorithms		
ImageJ	National Institutes of Health	https://1magej.nih.gov/1j/
LabChart	AD Instruments	https://www.adinstruments.com/products/labchart
iox2	emka Technologies	http://www.emka.fr/product/iox2-software/